Electronic Supplementary Material (ESI) for Journal of Materials Chemistry A.
This journal is © The Royal Society of Chemistry 2021

SUPPLEMENTARY INFORMATION

Large Areal Capacity and Dendrite-free Anode with Long Lifetime Enabled by Distributed Lithium Plating with Mossy Manganese Oxides

Jian Tan[1], Fernando A. Soto[2], Juran Noh[3], Peng Wu[3], Digvijay Rajendra Yadav[3], Kelvin Xie[3],

Perla B. Balbuena[2,3,4], Choongho Yu[1,3]*

[1] Department of Mechanical Engineering

[2] Department of Chemical Engineering

[3] Department of Materials Science and Engineering

[4] Department of Chemistry

Texas A&M University, College Station, Texas 77843 USA

*Corresponding author: chyu@tamu.edu

Supporting video S1. Testing of molten lithium infusion into MO-CNT.

Supporting video S2. Testing of molten lithium infusion into P-CNT.

Experimental Section

Preparation of CNT electrodes: 3D porous carbon nanotubes (CNTs) were synthesized by a chemical vapor deposition (CVD) method following our earlier work.[1, 2] A crucible filled with ~0.3 g ferrocene (Sigma-Aldrich, 98%) was placed in zone 1 (upstream) of a quartz tube whose inner diameter is ~22 mm. During the growth, hydrogen (Airgas, 99.999%), ethylene (Airgas, 99.999%), and argon (Airgas, 99.999%) gases were flowed into the tube at flow rates of 260 sccm, 80 sccm, and 80 sccm, respectively. The argon gas was passed through a bubbler filled with deionized (DI) water at room temperature. The furnace temperatures of zone 1, zone 2 and zone 3 (CNT growth zone) were 120 °C, 120 °C, and 650 °C, respectively.

Preparation of manganese oxide decorated CNT (MO-CNT) electrodes: MO-CNTs were synthesized by a facile hydrothermal reaction. 0.05M $KMnO_4$ (AMRESCO, >99%) solution was prepared in deionized (DI) water. The pH value of the solution was adjusted to 2 by adding HCl (Macron Fine Chemicals, 36.5%-38.0%). CNT slices and the reaction solution were pre-heated in a temperature-controlled oven at 90 °C for 30 min. The CNT slices were immersed into the solution and kept in the oven for 30 min. After the hydrothermal reaction, the CNT slices were taken out and rinsed with sufficient DI water. Finally, the MO-CNT was dried in the oven at 50 °C overnight before use. Typical sample thickness ranges from 200 to 500 μm.

In-operando pouch cell assembly and testing: In-operando cells were fabricated using pouch cell films with a cover glass (thickness No.1) as a viewing window (see Fig. S4). Copper foils wrapping around typical microscope glass slides (thickness: ~1 mm) were used as current collectors on top of another glass slide. CNT and lithium metal (Alfa Aesar, 99.9%) were placed in the middle with a Celgard 2400 separator in between, and then the two glass slides with the current collectors were pushed against each other. The amount of the electrolyte (1 M LiTFSI (Sigma-Aldrich, 99%) and 0.5 M $LiNO_3$ (Alfa Aesar, 99%) in a mixture of 1,3-dioxolane (Alfa Aesar, 99.5%) and 1,2-dimethoxyethane (Alfa Aesar, 99+%) (1:1 by vol.)) was 500 μL to fill in the pouch cell. All the lithium insertion processes were carried out with a constant current density of 1 mA/cm^2 without formation cycles. Dark-field optical microscope (Olympus BX5) images were taken every 1 minute using Q capture Pro program and made a video by an image merging program (Openshot Video editor).

Electrochemical impedance spectroscopy (EIS) measurement & analysis: EIS measurements were performed with Gamry 1010E electrochemical workstation and Arbin battery tester. The impedance spectra were recorded with an amplitude of 5 mV over the frequency range from 1 MHz to 0.01 Hz. The results were fitted to typical equivalent circuit with Gamry Echem Analyst. The real part of impedance (Z_{Re}) can be expressed as:

$$Z_{Re} = \delta\omega^{-1/2} \tag{1}$$

where δ is Warburg factor and ω (unit: Ω $s^{-0.5}$) is angular frequency (= $2\pi f$, where f is frequency). From the experimentally obtained relation between Z_{Re} and $\omega^{-1/2}$, δ can be found by linear fitting.

$$\delta = \frac{RT}{An^2F^2\sqrt{2}}\left(\frac{1}{\sqrt{D}C}\right) \tag{2}$$

where R is gas constant (8.314 J K^{-1} mol^{-1}), T is temperature (298 K), A is electrode area (0.7125 cm^2), n is reactant ratio, F is Faraday constant (96500 C mol^{-1}), D is diffusivity (cm^2 s^{-1}) and C is ion concentration (mol L^{-1}). Note that A is the area facing the lithium metal. C is the initial lithium ion concentration, 1.5 M, and n is 1 for lithium ion redox reaction ($Li^+ + e^- \rightarrow Li$ (metal)). EIS data were fitted using the equivalent circuit in Fig. S1. R_u refers the electrolyte solution resistance within the cell and the intrinsic resistance, including the contact resistance and the resistance within the active materials. R_p, Y0, and W_d, represent the contact resistance, constant phase element and Warburg coefficient, respectively.

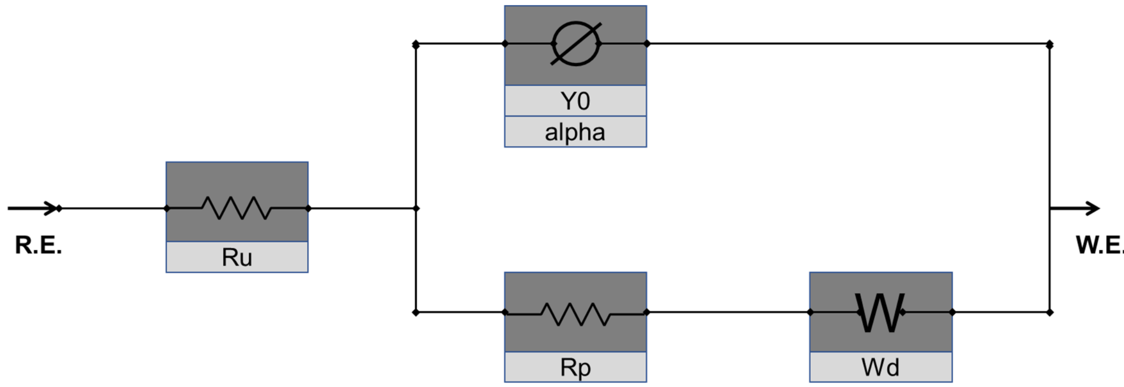

Figure S1. Equivalent circuit for EIS data.

Computational Methodology

Density functional theory (DFT) calculations were performed using the Vienna ab initio simulation package (VASP) code with the projector augmented wave (PAW) pseudopotentials.[3-6] Generalized gradient approximation (GGA) of Perdew–Burke–Ernzerhof (PBE) functionals were used to implement electron exchange-correlation interactions with a kinetic energy cutoff of 400 eV.[7] The van der Wals (vdW) interaction was described with DFT-D3 method.[8] The self-consistent field (SCF) and geometry convergence tolerance were set to 1×10^{-4} and 1×10^{-3} eV, respectively. A Γ-point-centered Monkhorst−Pack reciprocal grid of 3×5×2 k-points was used for first Brillouin zone sampling.[9] On-site Coulomb interactions were included by using the DFT+U formalism of Dudarev and co-workers.[10] For Mn atoms, an on-site coulomb interaction parameter of U = 3.9 eV was implemented.[11] To avoid interactions arising from periodic boundary conditions, a vacuum space greater than 10 Å was introduced in the normal direction.

To study the interaction of a CNT/MnO_2 system with Li, the CNT structure was approximated as a 12.78 Å × 7.38 Å planar single layer graphene structure. Meanwhile, the MnO_2 system was approximated as a Mn_8O_{16} cluster carved out from an optimized MnO_2 bulk system. Moreover, we used a 12.78 Å × 14.76 Å planar single layer graphene structure to calculate the binding energy of Li atoms onto this structure. The Li binding energies were calculated using the following equation:

$$E_B = \frac{(E_{Total} - E_{Substrate} - (n \times E_{Li}))}{n} \tag{3}$$

Here, E_{Total} is the energy of the total system, $E_{Substrate}$ is the energy of the unlithiated CNT or MO-CNT structure and E_{Li} is the calculated cohesive energy of Li (-1.60 eV) and n is the number of Li atoms inserted. To explore the interactions of the solvent with the bare CNT structure and the CNT/MnO_2 system, we conducted an interaction energy and charge density difference (CDD) analysis of a DOL solvent molecule interacting with both systems. The interaction energy (E_{IE}) is defined in the following way:

$$E_{IE} = (E_{Total} - E_{Slab} - E_{DOL}) \tag{4}$$

Here, E_{Total}, E_{Slab} and E_{DOL} represent the energy of the total system, the energy of the slab (without DOL molecule) and the energy of the DOL molecule, respectively.

Calculation of Areal Gibbs Free Energy

$$\text{Areal Gibbs free energy } \left(\mathrm{J}/\mathrm{m}^2\right) = \frac{\text{standard Gibbs free energy} \times \text{density}}{\text{molar mass}} \times \text{thickness}(t)$$

$$Li + 2MnO_2 = LiMn_2O_4 \tag{5}$$

$$Li + LiMn_2O_4 = 2LiMnO_2 \tag{6}$$

The standard Gibbs free energy at 298 K was calculated to be -469 kJ mol^{-1} and -332 kJ mol^{-1} for reaction (5) and (6), respectively. Thickness t (m).

$$\text{Areal Gibbs free energy for (5)} = \frac{-469(\text{kJ/mol}) \times 1000 \times 4.02(\text{g/cm}^3)}{108.8(\text{g/mol})} \times t \times 1000000$$

$$= -17.3 \times t \times 10^9(\text{J/m})$$

$$\text{Areal Gibbs free energy } for \text{ (6)} = \frac{-332(\text{kJ/mol}) \times 1000 \times 4.04(\text{g/cm}^3)}{93.9(\text{g/mol})} \times t \times 1000000$$

$$= -14.3 \times t \times 10^9(\text{J/m})$$

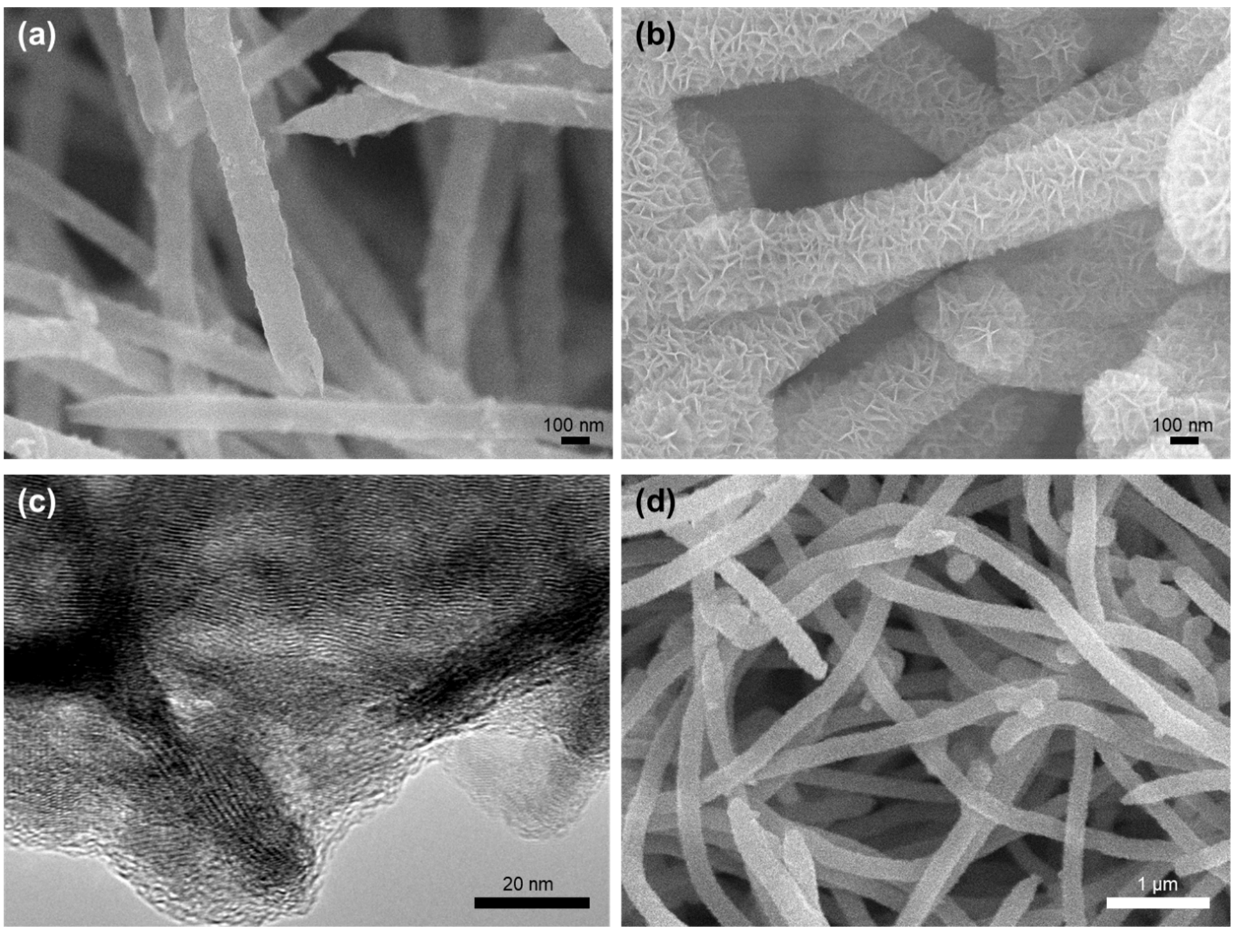

Figure S2. SEM image of (a) P-CNT and (b) MO-CNT, (c) TEM image of MO-CNT showing graphitic layer of CNT and polycrystalline grains of MnO_2, (d) SEM image of MO-CNT showing porous features after MnO_2 decoration on CNT.

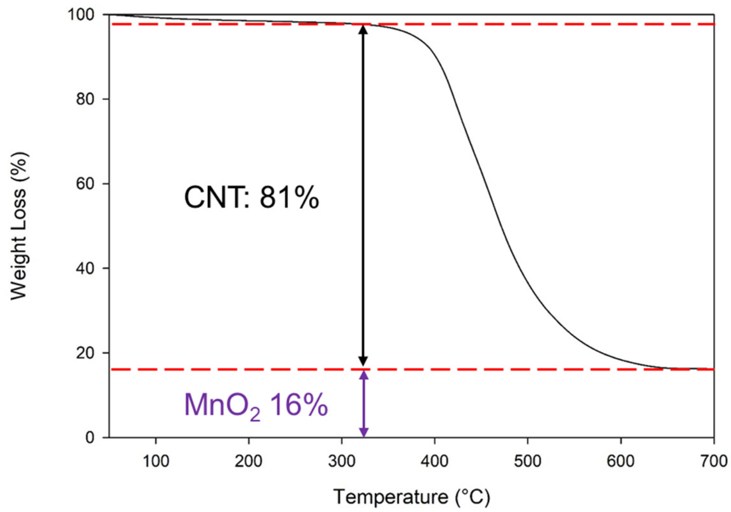

Figure S3. Thermogravimetric analysis (TGA) result of MO-CNT.

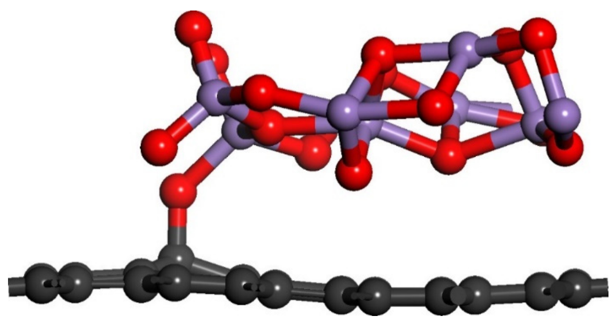

Figure S4. Geometry optimization of the CNT/MnO_2 system according to density functional theory (DFT) calculations at 0 K. Color code: black, red, and purple spheres represent C, O and Mn atoms, respectively.

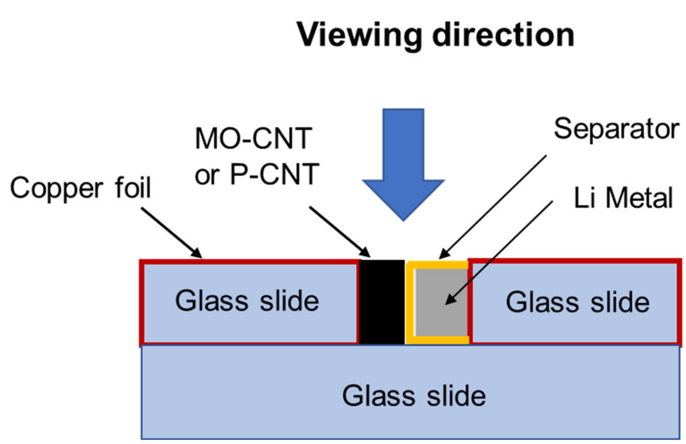

Figure S5. Schematic of the in-operando pouch cell setup.

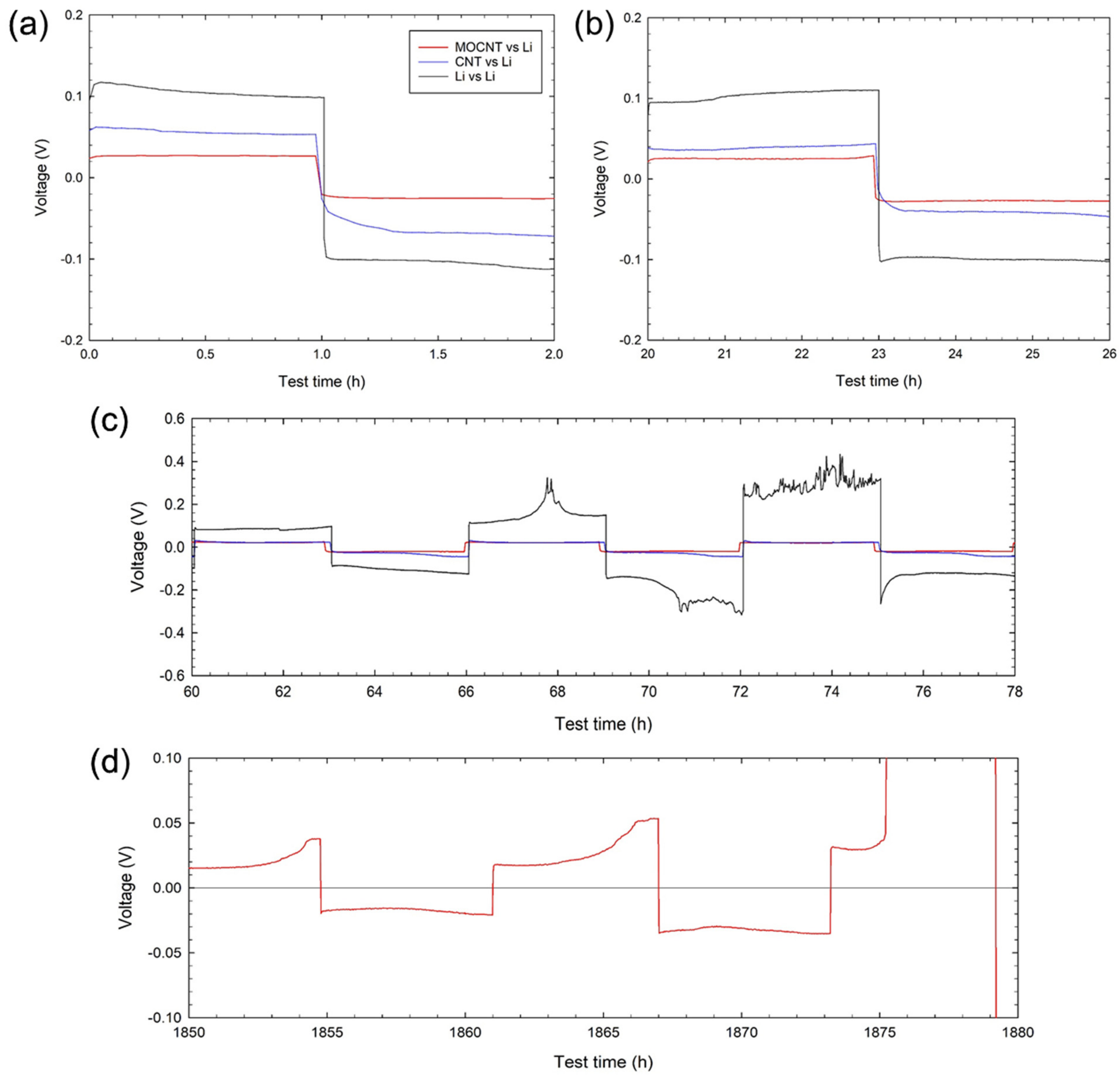

Figure S6. Voltage profiles of MO-CNT, P-CNT, and Li metal (with Li metal counter electrodes).

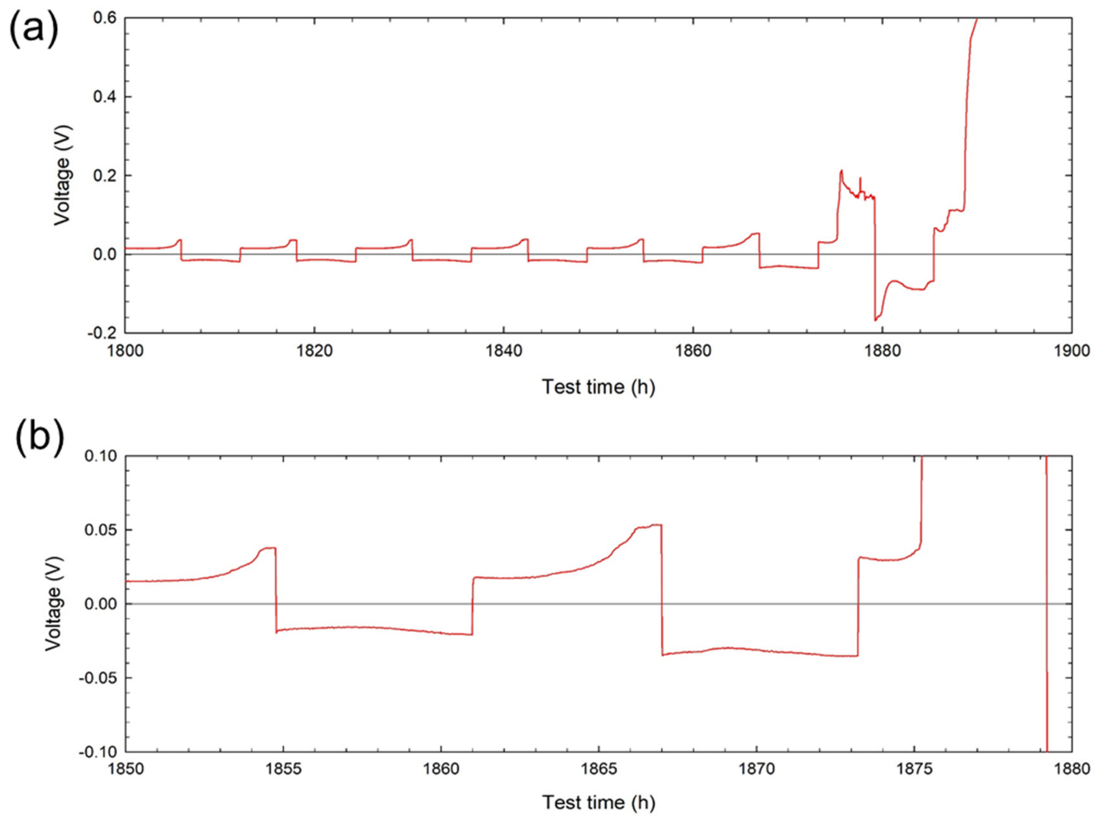

Figure S7. Voltage profiles of MO-CNT (vs Li metal counter electrode) near the failure cycles.

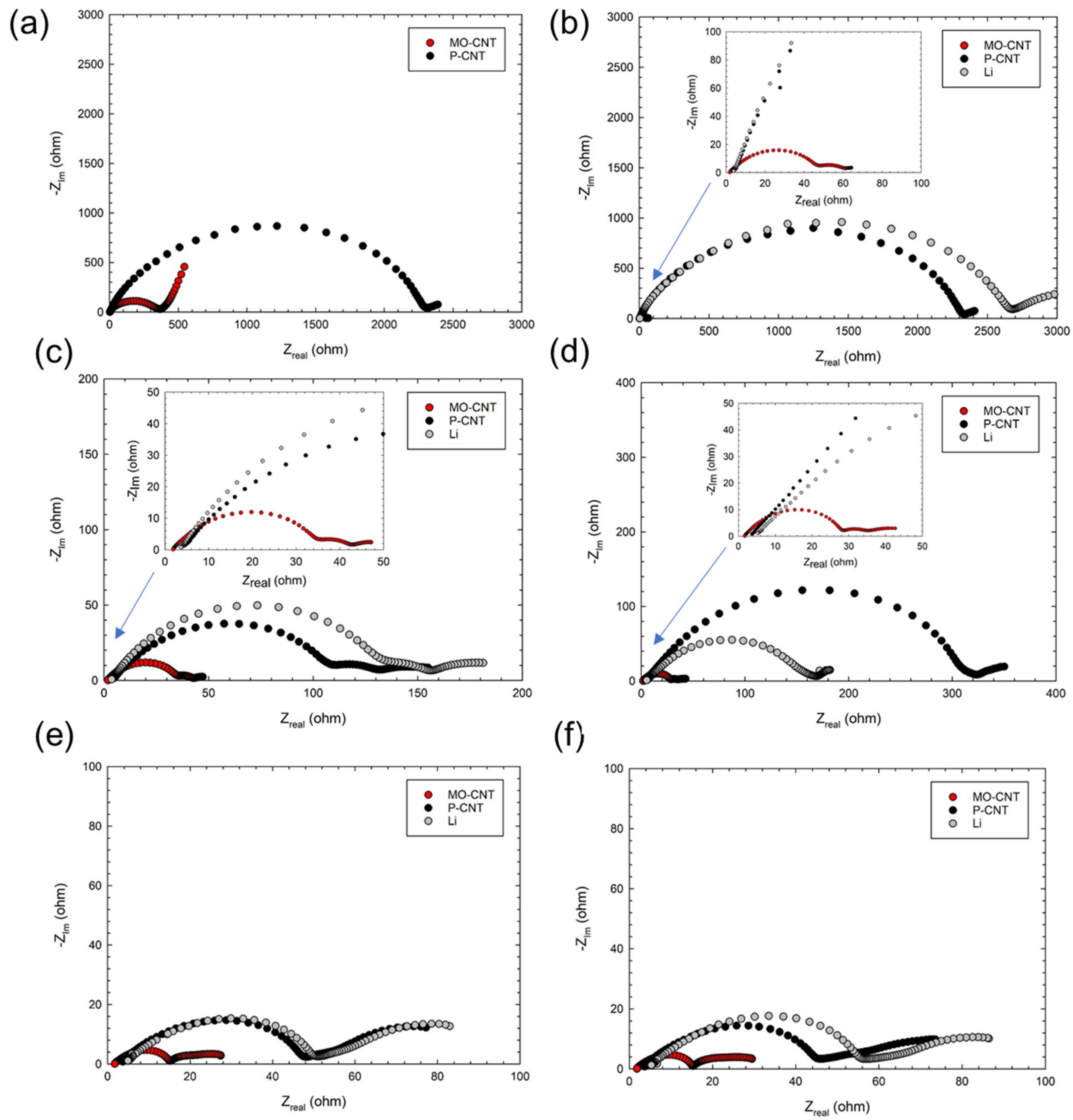

Figure S8. EIS analysis from step 1 to 6 (a-f).

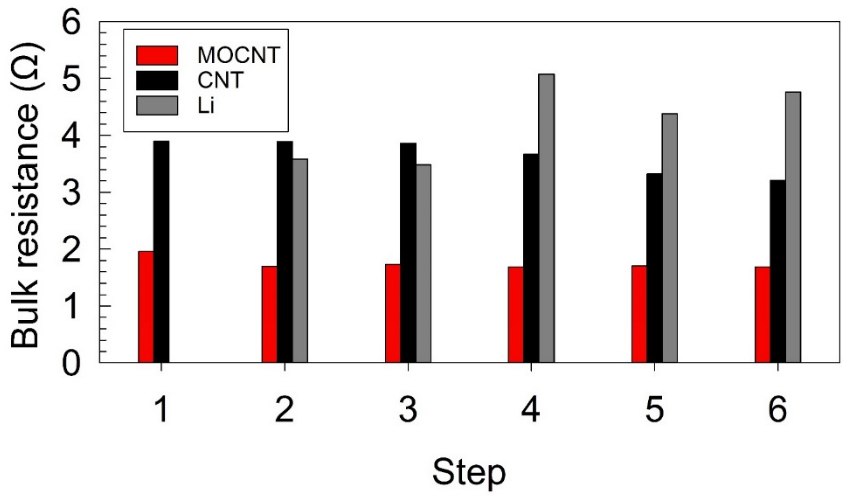

Figure S9. Bulk resistance at the stages of (1) before lithiation, (2) after full lithiation, (3) plating of Li up to 8 mAh/cm^2, after a stripping/plating cycle with capacities of (4) 1 mAh/cm^2, (5) 3 mAh/cm^2, and (6) 6 mAh/cm^2.

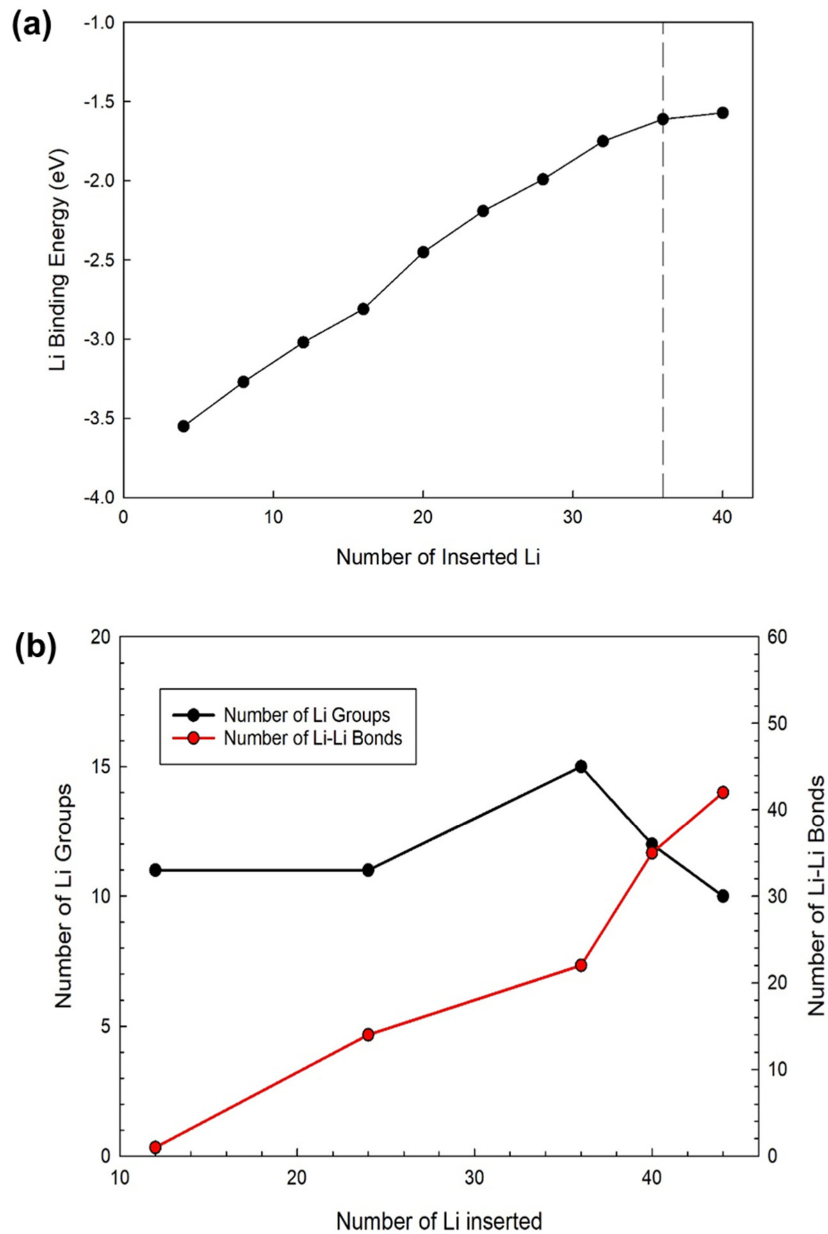

Figure S10. (a) Binding energy (eV) profile of the sequential Li insertion in the CNT/MnO_2 system. (b) Number of isolated Li groups and number of Li-Li bonds as a function of Li inserted in the system.

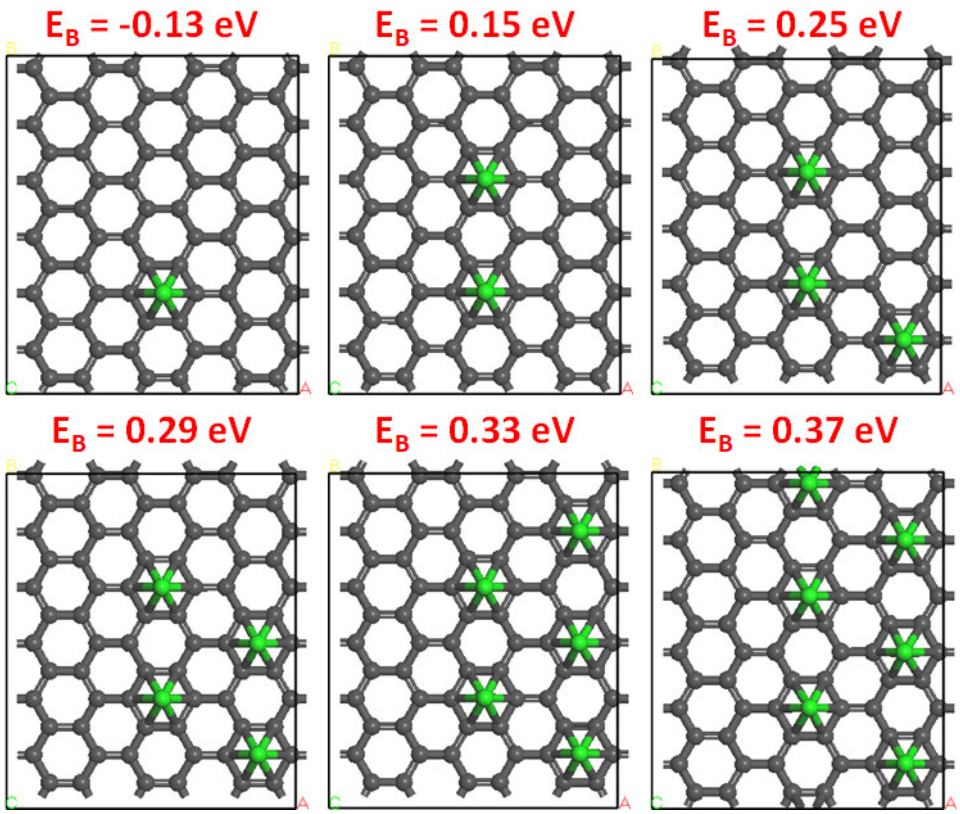

Figure S11. The optimized geometry and binding energy (E_B) of six Li atoms deposited on a bare graphene structure. Color code: black and green spheres represent C and Li atoms, respectively.

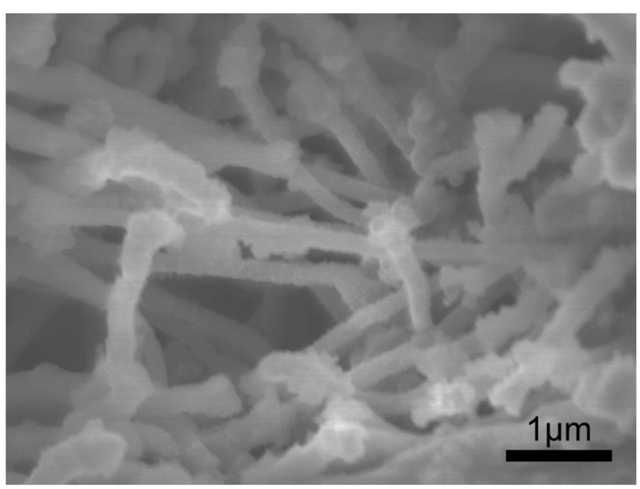

Figure S12. A SEM image of a cross-section of MO-CNT electrode after cycling.

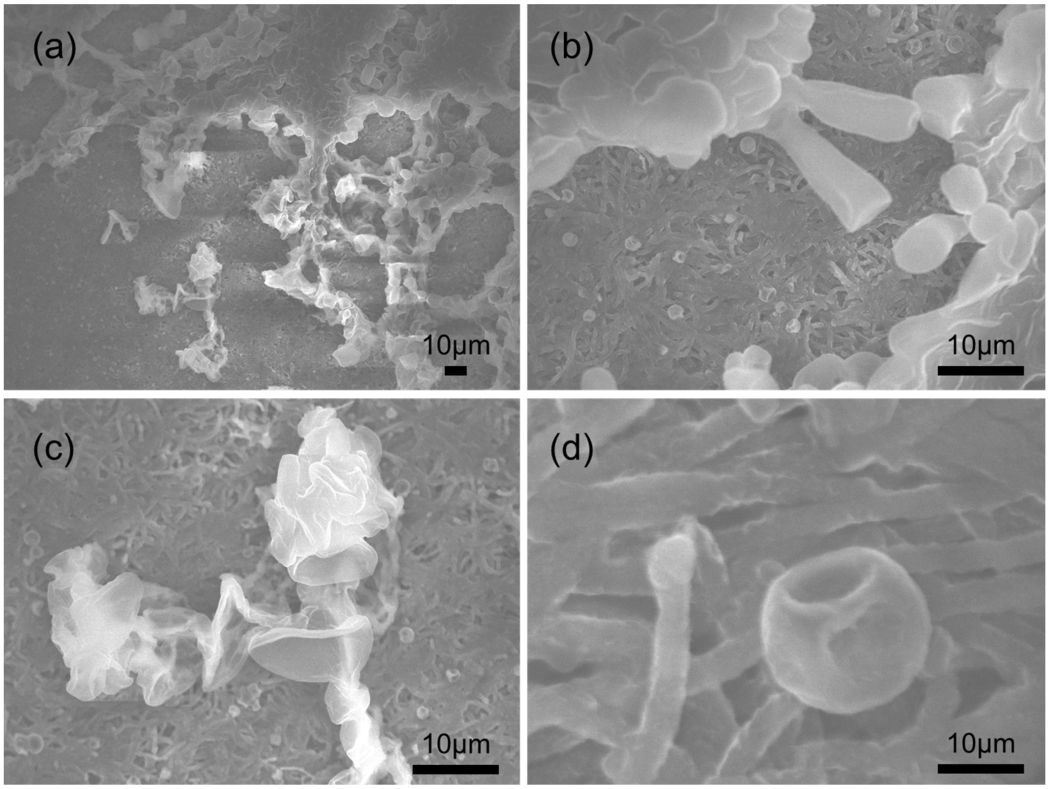

Figure S13. SEM images of Li dendrites deposited on P-CNT surface.

Table S1. Literature comparison.

Material	Areal capcity (mAh/cm2)	Cycle number	Time per cycle (hours)	Areal capacity × Lifetime	Catalog	Symbol	Ref
This work	6	150	12	10800	Carbon-based	★	
Hollow carbon fiber	2	350	8	5600	Carbon-based	●	12
CNT Sponge	2	90	4	720	Carbon-based	⬢	13
MO @ Graphene	1	800	2	1600	Carbon-based	◓	14
Graphite	3.35	37	4	502.5	Carbon-based	▲	15
Au-embedded GO	4	600	2	4800	Carbon-based	■	16
MOF@Carbon cloth	5	800	1	4000	Carbon-based	▼	17
Si@Carbon	1	1000	1	1000	Carbon-based	◆	18
Carbon paper	2	500	2	2000	Carbon-based	◀	18
Carbon microtube skeleton	2	250	4	2000	Carbon-based	+	19
Carbon/Si	1	80	0.67	53.6	Carbon-based	◐	20
Carbon/CuO	1	500	2	1000	Carbon-based	◑	21
N-doped Carbon	1	1200	1	1200	Carbon-based	◒	22
Ni @ Carbon fiber	2	125	4	1000	Carbon-based	⬒	23
Amine @ CNT	1	250	2	500	Carbon-based	⬓	24
N-doped Graphene	1	727	2	1454	Carbon-based	◪	25
Al @ Cu	1	1700	4	6800	Metal-based	●	26
Cu	5	80	10	4000	Metal-based	▲	27
Cu	3	300	0.6	540	Metal-based	◑	28

Cu	2	130	8	2080	Metal-based		29
Cu2O @ Cu	1	500	2	1000	Metal-based		30
ZnO @ Ni foam	1	400	2	800	Metal-based		31
Zn	2	1	800	1600	Metal-based		32
Cu foam	1	280	2	560	Metal-based		33
Vertical Cu Channels	1	100	2	200	Metal-based		34
Cu/CuO	1	500	2	1000	Metal-based		35
Tin-Li alloy	5	200	2	400	Metal-based		36
ZnO @ PI	1	100	2	200	Polymer		37
PAN	1	200	2	400	Polymer		38
Reinforced Li	8.8	200	1	1760	Conductive Polymer		39
Polymer	9.5	250	1	2375	Polymer		40
MoS2 Coating	1	150	2	300	SEI		41
MCI	0.5	2000	0.4	400	SEI		42
SEI	1	120	2	240	SEI		43
SEI	1	581	4	2325	SEI		44
Metal chloride perovskite	1	400	2	800	SEI		45
SEI	1.8	250	2	900	SEI		46
Polymer SEI	1	200	2	400	SEI		38
Separator	0.25	1000	0.5	500	Separator		47
nano-LiF@polymer hybrid SICs	2	500	2	1000	Separator		48
Si@Li	1	1500	1	1500	Si-Membrane		49
MOF@Carbon cloth	5	1000	1	5000	MOF		17
MOF@Carbon fiber	1	1000	1	1000	MOF		50
Polymer	0.2	200	4	160	Polymer		51

References

1. G. Yang, W. Choi, X. Pu and C. Yu, *Energy & Environmental Science*, 2015, **8**, 1799-1807.
2. G. Yang, J. Tan, H. Jin, Y. H. Kim, X. Yang, D. H. Son, S. Ahn, H. Zhou and C. Yu, *Advanced Functional Materials*, 2018, **28**, 1800595.
3. G. Kresse and J. Hafner, *Physical Review B*, 1993, **47**, 558-561.
4. G. Kresse and J. Hafner, *Physical Review B*, 1994, **49**, 14251-14269.
5. G. Kresse and J. Furthmüller, *Computational Materials Science*, 1996, **6**, 15-50.
6. G. Kresse and J. Furthmüller, *Physical Review B*, 1996, **54**, 11169-11186.
7. J. P. Perdew, K. Burke and M. Ernzerhof, *Physical Review Letters*, 1996, **77**, 3865-3868.
8. S. Grimme, J. Antony, S. Ehrlich and H. Krieg, *The Journal of Chemical Physics*, 2010, **132**, 154104.
9. H. J. Monkhorst and J. D. Pack, *Physical Review B*, 1976, **13**, 5188-5192.
10. S. L. Dudarev, G. A. Botton, S. Y. Savrasov, C. J. Humphreys and A. P. Sutton, *Physical Review B*, 1998, **57**, 1505-1509.
11. A. L. Dzubak, C. Mitra, M. Chance, S. Kuhn, G. E. JellisonJr., A. S. Sefat, J. T. Krogel and F. A. Reboredo, *The Journal of Chemical Physics*, 2017, **147**, 174703.
12. L. Liu, Y.-X. Yin, J.-Y. Li, N.-W. Li, X.-X. Zeng, H. Ye, Y.-G. Guo and L.-J. Wan, *Joule*, 2017, **1**, 563-575.
13. G. Yang, Y. Li, Y. Tong, J. Qiu, S. Liu, S. Zhang, Z. Guan, B. Xu, Z. Wang and L. Chen, *Nano Letters*, 2019, **19**, 494-499.
14. B. Yu, T. Tao, S. Mateti, S. Lu and Y. Chen, *Advanced Functional Materials*, 2018, **28**, 1803023.
15. Y. Son, T. Lee, B. Wen, J. Ma, C. Jo, Y.-G. Cho, A. Boies, J. Cho and M. De Volder, *Energy & Environmental Science*, 2020, DOI: 10.1039/D0EE02230F.
16. T. Yang, L. Li, F. Wu and R. Chen, *Advanced Functional Materials*, 2020, **30**, 2002013.
17. T. Zhou, J. Shen, Z. Wang, J. Liu, R. Hu, L. Ouyang, Y. Feng, H. Liu, Y. Yu and M. Zhu, *Advanced Functional Materials*, 2020, **30**, 1909159.
18. Y. An, Y. Tian, H. Wei, B. Xi, S. Xiong, J. Feng and Y. Qian, *Advanced Functional Materials*, 2020, **30**, 1908721.
19. C. Sun, T. Wu, J. Wang, W. Li, J. Jin, J. Yang and Z. Wen, *Journal of Materials Chemistry A*, 2018, **6**, 19159-19166.
20. Z. Liang, D. Lin, J. Zhao, Z. Lu, Y. Liu, C. Liu, Y. Lu, H. Wang, K. Yan, X. Tao and Y. Cui, *Proceedings of the National Academy of Sciences*, 2016, **113**, 2862.
21. X.-Y. Yue, X.-L. Li, W.-W. Wang, D. Chen, Q.-Q. Qiu, Q.-C. Wang, X.-J. Wu, Z.-W. Fu, Z. Shadike, X.-Q. Yang and Y.-N. Zhou, *Nano Energy*, 2019, **60**, 257-266.
22. L. Liu, Y.-X. Yin, J.-Y. Li, S.-H. Wang, Y.-G. Guo and L.-J. Wan, *Advanced Materials*, 2018, **30**, 1706216.
23. J. Chang, J. Shang, Y. Sun, L. K. Ono, D. Wang, Z. Ma, Q. Huang, D. Chen, G. Liu, Y. Cui, Y. Qi and Z. Zheng, *Nature Communications*, 2018, **9**, 4480.
24. C. Niu, H. Pan, W. Xu, J. Xiao, J.-G. Zhang, L. Luo, C. Wang, D. Mei, J. Meng, X. Wang, Z. Liu, L. Mai and J. Liu, *Nature Nanotechnology*, 2019, **14**, 594-601.
25. G. Huang, J. Han, F. Zhang, Z. Wang, H. Kashani, K. Watanabe and M. Chen, *Advanced Materials*, 2019, **31**, 1805334.

26. H. Ye, Z.-J. Zheng, H.-R. Yao, S.-C. Liu, T.-T. Zuo, X.-W. Wu, Y.-X. Yin, N.-W. Li, J.-J. Gu, F.-F. Cao and Y.-G. Guo, *Angewandte Chemie International Edition*, 2019, **58**, 1094-1099.
27. Z. Cao, B. Li and S. Yang, *Advanced Materials*, 2019, **31**, 1901310.
28. S. Wu, T. Jiao, S. Yang, B. Liu, W. Zhang and K. Zhang, *Journal of Materials Chemistry A*, 2019, **7**, 5726-5732.
29. P. Zou, Y. Wang, S.-W. Chiang, X. Wang, F. Kang and C. Yang, *Nature Communications*, 2018, **9**, 464.
30. Y. Ma, Y. Gu, Y. Yao, H. Jin, X. Zhao, X. Yuan, Y. Lian, P. Qi, R. Shah, Y. Peng and Z. Deng, *Journal of Materials Chemistry A*, 2019, **7**, 20926-20935.
31. F. Zhao, X. Zhou, W. Deng and Z. Liu, *Nano Energy*, 2019, **62**, 55-63.
32. J. Kim, J. Lee, J. Yun, S. H. Choi, S. A. Han, J. Moon, J. H. Kim, J.-W. Lee and M.-S. Park, *Advanced Functional Materials*, 2020, **30**, 1910538.
33. X. Ke, Y. Cheng, J. Liu, L. Liu, N. Wang, J. Liu, C. Zhi, Z. Shi and Z. Guo, *ACS Applied Materials & Interfaces*, 2018, **10**, 13552-13561.
34. S.-H. Wang, Y.-X. Yin, T.-T. Zuo, W. Dong, J.-Y. Li, J.-L. Shi, C.-H. Zhang, N.-W. Li, C.-J. Li and Y.-G. Guo, *Advanced Materials*, 2017, **29**, 1703729.
35. X.-Y. Yue, W.-W. Wang, Q.-C. Wang, J.-K. Meng, X.-X. Wang, Y. Song, Z.-W. Fu, X.-J. Wu and Y.-N. Zhou, *Energy Storage Materials*, 2019, **21**, 180-189.
36. M. Wan, S. Kang, L. Wang, H.-W. Lee, G. W. Zheng, Y. Cui and Y. Sun, *Nature Communications*, 2020, **11**, 829.
37. Y. Liu, D. Lin, Z. Liang, J. Zhao, K. Yan and Y. Cui, *Nature Communications*, 2016, **7**, 10992.
38. J. Bae, Y. Qian, Y. Li, X. Zhou, J. B. Goodenough and G. Yu, *Energy & Environmental Science*, 2019, **12**, 3319-3327.
39. J.-H. Kim, Y.-H. Lee, S.-J. Cho, J.-G. Gwon, H.-J. Cho, M. Jang, S.-Y. Lee and S.-Y. Lee, *Energy & Environmental Science*, 2019, **12**, 177-186.
40. T. Dong, J. Zhang, G. Xu, J. Chai, H. Du, L. Wang, H. Wen, X. Zang, A. Du, Q. Jia, X. Zhou and G. Cui, *Energy & Environmental Science*, 2018, **11**, 1197-1203.
41. E. Cha, M. D. Patel, J. Park, J. Hwang, V. Prasad, K. Cho and W. Choi, *Nature Nanotechnology*, 2018, **13**, 337-344.
42. C. Yan, X.-B. Cheng, Y.-X. Yao, X. Shen, B.-Q. Li, W.-J. Li, R. Zhang, J.-Q. Huang, H. Li and Q. Zhang, *Advanced Materials*, 2018, **30**, 1804461.
43. X. Shen, Y. Li, T. Qian, J. Liu, J. Zhou, C. Yan and J. B. Goodenough, *Nature Communications*, 2019, **10**, 900.
44. R. Pathak, K. Chen, A. Gurung, K. M. Reza, B. Bahrami, J. Pokharel, A. Baniya, W. He, F. Wu, Y. Zhou, K. Xu and Q. Qiao, *Nature Communications*, 2020, **11**, 93.
45. Y.-C. Yin, Q. Wang, J.-T. Yang, F. Li, G. Zhang, C.-H. Jiang, H.-S. Mo, J.-S. Yao, K.-H. Wang, F. Zhou, H.-X. Ju and H.-B. Yao, *Nature Communications*, 2020, **11**, 1761.
46. J.-Y. Hwang, S.-J. Park, C. S. Yoon and Y.-K. Sun, *Energy & Environmental Science*, 2019, **12**, 2174-2184.
47. M. M. U. Din and R. Murugan, *Scientific Reports*, 2019, **9**, 16795.
48. C. Fu, V. Venturi, J. Kim, Z. Ahmad, A. W. Ells, V. Viswanathan and B. A. Helms, *Nature Materials*, 2020, **19**, 758-766.
49. T. Xu, P. Gao, P. Li, K. Xia, N. Han, J. Deng, Y. Li and J. Lu, *Advanced Energy Materials*, 2020, **10**, 1902343.

50. G. Jiang, N. Jiang, N. Zheng, X. Chen, J. Mao, G. Ding, Y. Li, F. Sun and Y. Li, *Energy Storage Materials*, 2019, **23**, 181-189.
51. Y. He, H. Xu, J. Shi, P. Liu, Z. Tian, N. Dong, K. Luo, X. Zhou and Z. Liu, *Energy Storage Materials*, 2019, **23**, 418-426.